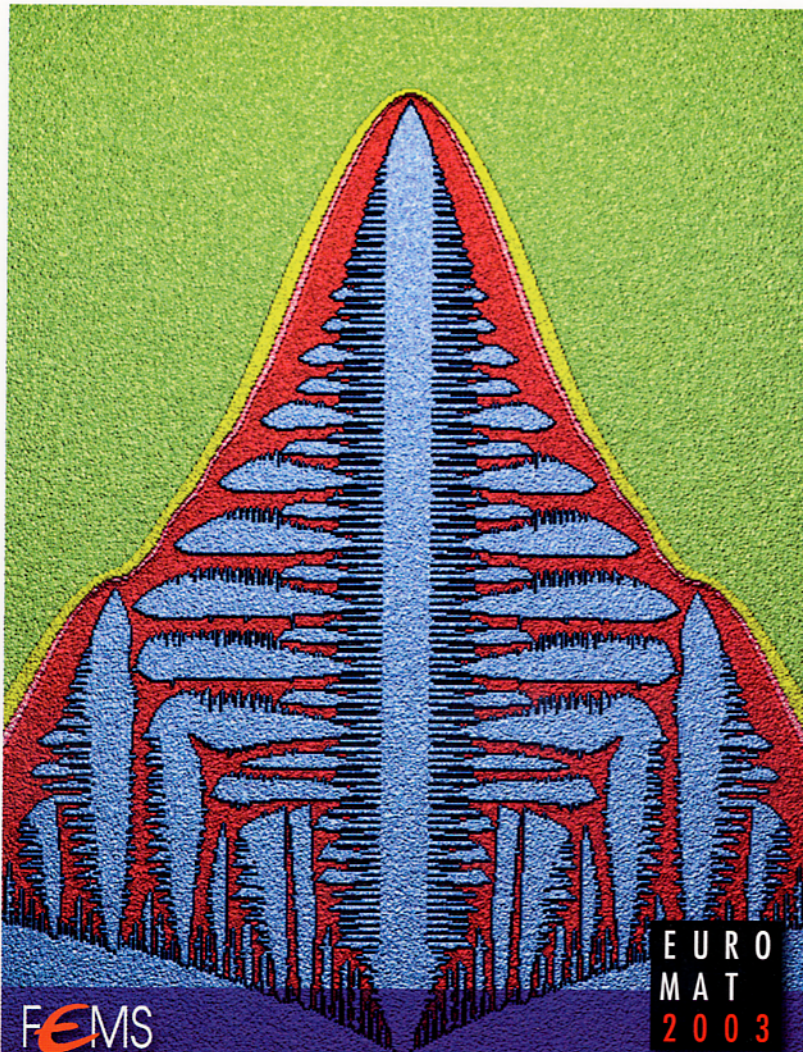


Edited by Dieter M. Herlach

WILEY-VCH

Solidification and Crystallization



EUROMAT
Publications

EURO
MAT
2003

7

Phase-Field Modeling of Dendritic Solidification: Verification for the Model Predictions with Latest Experimental Data

P.K. GALENKO, D.M. HERLACH, O. FUNKE, G. PHANIKUMAR

Abstract

The results on modeling of dendritic solidification from undercooled melts are discussed. In order to model the details of formation of dendritic patterns we use a phase-field model of dendritic growth in a pure undercooled system with convection of the liquid phase. The predictions of the phase-field model are discussed referring to our latest high accuracy measurements of dendrite growth velocities in nickel samples. Special emphasis is given to the growth of dendrites at small and moderate undercoolings. At small undercoolings, the theoretical predictions deviate systematically from experimental data for solidification of nickel dendrites.

7.1

Introduction

Since several decades now dendritic growth velocities V have been measured during solidification of electromagnetically levitated metal melts. Different techniques have been applied, e.g. the usage of a fast responding photo-double-diode [1,2] or an ultra-high-speed camera system [3]. Following the sharp interface model of dendrite growth by Kurz et al. (LGK/LKT model) [4,5], the prediction of the dendritic growth velocity V as a function of the undercooling ΔT is in good agreement with experimental data for nickel solidification only in the region of medium undercoolings $100 \text{ K} < \Delta T < 200 \text{ K}$ [2]. Recently, we suggested a modification to the sharp interface LGK/LKT model which takes into account the effect of forced convective flow caused by electromagnetic stirring [6]. It is shown that this modification leads to an increase of the calculated velocity when the melt flow is opposite to the direction of the steady-state dendritic growth. However, the effect of forced convective flow alone can still not explain the measured data in a satisfying manner [6]. Therefore, (i) we essentially improved the accuracy of the technique and performed new measurements of dendritic growth velocities in levitated undercooled nickel samples (see Ref. [7] and references therein), and, in the present work, (ii) we present the phase-field model predictions in comparison with the new measurements of dendrite growth ve-

locity measurements for levitated undercooled Ni melts obtained with an advanced capacitance proximity sensor (CPS) technique.

7.2

Governing equations

The phase-field model was suggested and developed for the description of phase transitions in condensed matter with diffuse phase interfaces (see, e.g., overviews in Refs. [8,9]). In the present investigation, we have used the “thin-interface” analysis of the phase-field model [10,11] where the interface thickness W_0 is assumed to be small compared to the scale of the crystal but not smaller than the microscopic capillary length d_0 . The thin-interface limit is ideally suited to model dendritic growth in pure materials quantitatively at low undercoolings when used in conjunction with efficient numerical algorithms [12]. The phase-field and energy equations were taken from the model of Karma and Rappel [10,11] with the momentum and continuity equations of motion of the liquid phase taken from Beckermann et al. [13]. Furthermore, in the momentum equation, the additional force for the motion of the liquid phase in an undercooled levitated droplet, i.e. the Lorentz force $\vec{F}_{LZ} = c^{-1} \vec{J} \times \vec{B}$ caused by the alternating electromagnetic field, has been introduced (here c is the speed of light, \vec{J} is the electric current density, and \vec{B} is the vector of magnetic induction).

The main governing equations are described by

– *energy conservation*

$$\frac{\partial T}{\partial t} + (1 - \varphi)(\vec{v} \cdot \nabla)T = a\nabla^2 T + \frac{T_Q}{2} \frac{\partial \Phi}{\partial t}, \quad (1)$$

– *continuity of the liquid phase*

$$\nabla \cdot [(1 - \varphi)\vec{v}] = 0, \quad (2)$$

– *momentum transfer*

$$(1 - \varphi)(\vec{v} \cdot \nabla)\vec{v} = -\frac{1 - \varphi}{\rho}\nabla p + \frac{(1 - \varphi)}{\rho}\vec{F}_{LZ} + \nabla \cdot [v\nabla(1 - \varphi)\vec{v}] + \vec{F}_D, \quad (3)$$

– *phasefield evolution*

$$\tau(\vec{n}) \frac{\nabla \Phi}{\partial t} = \nabla \cdot (W^2(\vec{n})\nabla \Phi) + \sum_{w=x,y,z} \frac{\partial}{\partial w} \left(|\nabla \Phi|^2 W(\vec{n}) \frac{\partial W(\vec{n})}{\partial (\partial_w \Phi)} \right) - \frac{\partial F}{\partial \Phi}. \quad (4)$$

In Eqs. (1)–(4) the following notations are accepted: T is the temperature, T_Q is the adiabatic temperature of solidification defined by $T_Q = Q/c_p$, Q and c_p are the la-

tent heat of solidification and specific heat per unit volume, respectively, Φ is the phase-field variable ($\Phi = -1$ is the liquid phase and $\Phi = 1$ is for the solid phase); $\varphi = (1 + \Phi)/2$ is the fraction of the solid phase ($\varphi = 0$ is for the liquid and $\varphi = 1$ is for the solid), \vec{v} is the fluid flow velocity in the liquid, x, y, z are the Cartesian coordinates, t is the time, a is the thermal diffusivity, ρ is the density, p is the pressure, and ν is the kinematic viscosity of the liquid phase. The dissipative force in the Navier-Stokes equation (3) is defined by $\vec{F}_D = -2\nu h\varphi^2(1 - \varphi^2)\vec{v}/W_0^2$, where the constant $h = 2.757$ is defined by the asymptotic analysis in Ref. [13]. Furthermore, in the solution of Eq. (3), the Lorentz force has been averaged in time: $\vec{F}_{LZ} \approx |B|^2/(4\pi\delta)$, where $|B| = B_o \cdot \exp[(r - R_o)/\delta]$ is the modulus of the magnetic induction vector, B_o is the time averaged value of the magnetic induction, r is the radial distance of a droplet of radius R_o , $\delta = [2/(\omega\sigma_R\mu_0)]^{1/2}$ is considered as a skin depth for the alternating magnetic field in the liquid droplet, which decreases for a short distance at which the modulus of magnetic induction $|B|$ decays exponentially, σ_R is the electric conductivity (measured under isothermal conditions), μ_0 is the magnetic permeability, and ω is the frequency of the applied current. The phenomenological free energy F is defined by $F(T, \Phi) = f(\Phi) + \lambda(T - T_M)g(\Phi)/T_Q$. With including the double-well function $f(\Phi) = -\Phi^2/2 + \Phi^4/4$ and the odd function $g(\Phi) = \Phi - 2\Phi^3/3 + \Phi^5/5$ itself, the form of the free energy F is constructed in such a way that a tilt λ of an energetic well controls the coupling between the fields of T and Φ .

The time $\tau(\vec{n})$ of the phase-field kinetics and the thickness $W(\vec{n})$ of the anisotropic interface are given by

$$\tau(\vec{n}) = \tau_0 a_c(\vec{n}) a_k(\vec{n}) \left[1 + a_2 \frac{\lambda d_0}{a\beta_0} \frac{a_c(\vec{n})}{a_k(\vec{n})} \right], \quad W(\vec{n}) = W_0 a_c(\vec{n}), \quad (5)$$

where τ_0 is the time-scale for the phase-field kinetics, W_0 is the parameter of the interface thickness with $W_0 = \lambda d_0/a_1$, and $a_1 = 5\sqrt{2}/8$. The second term in square brackets of Eq. (5) for $\tau(\vec{n})$ defines a correction for the “thin-interface” asymptotics with adopting a constant $a_2 = 0.6267$ [12] in comparison with the sharp-interface analysis. The functions $a_c(\vec{n})$ and $a_k(\vec{n})$ of interfacial anisotropy are described by

– the anisotropy of interfacial energy

$$a_c(\vec{n}) = \frac{\gamma(\vec{n})}{\gamma_0} = (1 - 3\varepsilon_c) \left[1 + \frac{4\varepsilon_c}{1 - 3\varepsilon_c} (n_x^4 + n_y^4 + n_z^4) \right], \quad (6)$$

where $\gamma(\vec{n})$ is the surface energy dependent on the normal vector \vec{n} to the interface, γ_0 is the mean value of the interfacial energy along the interface, and ε_c is the anisotropy parameter,

– the anisotropy of kinetics of atomic attachment to the interface

$$a_k(\vec{n}) = \frac{\beta(\vec{n})}{\beta_0} = (1 + 3\varepsilon_k) \left[1 - \frac{4\varepsilon_k}{1 + 3\varepsilon_k} (n_x^4 + n_y^4 + n_z^4) \right], \quad (7)$$

where $\beta(\vec{n})$ is the kinetic coefficient dependent on the normal vector \vec{n} to the interface, β_0 is the averaged kinetic coefficient along the interface which is defined by $\beta_0 = (\mu_{100} - \mu_{110})/(2 T_Q)$, and ε_k is the kinetic anisotropy parameter defined as $\varepsilon_k = (\mu_{100} - \mu_{110})/(\mu_{100} + \mu_{110})$. In Eqs. (5)–(7), the normal vector $\vec{n} = \vec{n}(n_x, n_y, n_z)$ has the components defined by the gradients of the phase-field as follows

$$n_x^4 + n_y^4 + n_z^4 = \frac{(\partial\Phi/\partial x)^4 + (\partial\Phi/\partial y)^4 + (\partial\Phi/\partial z)^4}{|\nabla\Phi|^4} \quad (8)$$

7.3

Results and Discussion

Equations (1)–(8) have been solved numerically by a finite-difference technique on a uniform computational grid with application of the special numerical algorithms. Particularly, we used the multi-grid algorithm for resolving the equations of the phase-field (4), heat transfer (1) and momentum (3) which have the different spatial lengths and time scales of their dynamics. The details of numerical algorithm and computational procedure of solution of dendritic growth with convective flow were the same as given in Refs. [14,15]. Parameters of modeling applicable to pure nickel are given in Table 1. The phase-field modeling of dendritic patterns has been carried out on Workstation – SUN BLADE 1000.

Tab. 1 Material's parameters for pure nickel and characteristics of the electromagnetic facility

Parameter	Symbol	Numerical value
Equilibrium temperature of solidification	T_M	1728 (K)
Latent heat of solidification	Q	$8.113 \cdot 10^9$ (J/m ³)
Specific heat	c_p	$1.939 \cdot 10^7$ (J/K/m ³)
Interface energy	γ_0	0.326 (J/m ²)
Capillary length	d_0	$1.66 \cdot 10^{-10}$ (m)
Interfacial kinetic coefficient in <100>-direction	μ_{100}	0.52 (m/s/K)
Interfacial kinetic coefficient in <110>-direction	μ_{110}	0.40 (m/s/K)
Density	ρ	8.110^3 (kg/m ³)
Dynamic viscosity	μ	4.310^{-3} (Pa · s)
Thermal diffusivity	a	$1.2 \cdot 10^{-5}$ (m ² /s)
Anisotropy constant	σ_0	1.1 (–)
Parameter of anisotropy	ε	1.810^{-2} (–)
Electric conductivity	σ_R	$4.1 \cdot 10^6$ ($\Omega \cdot m$)
Magnetic permeability	μ_0	$4 \cdot \pi \cdot 10^{-7}$ (H/m)
Frequency of the applied current	ω	$3.0 \cdot 10^5$ (1/s)

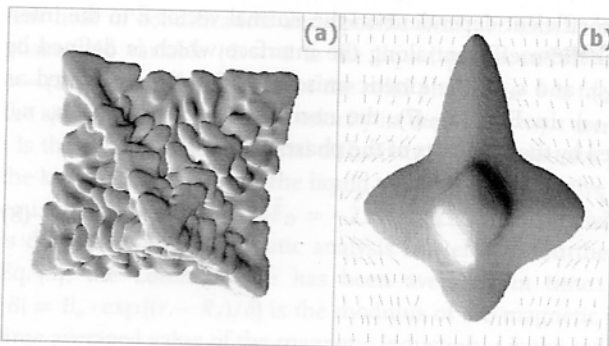


Fig. 1 (a) Dendritic growth pattern with side-branches due to application of finite level of thermal stochastic noise according to Ref. [16]. Dendrite has been obtained for pure nickel with the finite anisotropies of the interfacial energy and kinetics (see Table 1) at the undercooling $\Delta T = 0.55T_Q$. Pattern has been simulated on a grid of size 650^3 nodes. (b) Growth of nickel dendrite under convective flow at $T = 0.30T_Q$ and $U_0 = 0.7$ m/s. Growth velocity V of the up-stream branch is most pronounced in comparison with the down-stream branch due to forced convection with the far field flow speed U_0 . The speed U_0 has been found from the energy balance within the levitated droplet from Eq. (3) of Ref. [6] and with the parameters of the electromagnetic facility given in Table 1. Dashed lines around the dendrite indicate the flow velocity vectors in the vertical cross-section. Pattern has been simulated on a grid of size $230 \times 330 \times 330$ nodes.

7.3.1

Dendritic Patterns

Solution of the phase-field equations allows us to obtain the complete morphological spectrum of interfacial crystal structures for a wide range of undercoolings. In our modeling, the complete morphological spectrum of the crystal structures has been obtained, which exhibits a crystal changing from grained crystals at very small undercoolings ($\Delta T < 0.15 T_Q$) up to grained crystals at higher undercoolings ($\Delta T < 1.00 T_Q$) via the dendritic growth form within intermediate region. Therefore, within the range of undercoolings investigated $0.10 T_Q \leq \Delta T \leq 1.3 T_Q$, the growth form of dendrites is dictated by the preferable crystallographic direction. In addition to this, stochastic noise plays a crucial role in the formation of branched crystal patterns of dendritic type. Figure 1(a) shows the dendritic crystal with secondary and even tertiary branches with the application of the thermal noise. With no convective flow, dendrites grow in the stagnant melt in a symmetrical manner with the main stems growing along the preferable crystallographic directions of a crystal. Solidification under the influence of convective flow forced by electromagnetic stirring in a droplet, however produces dendritic growth strongly pronounced in the direction opposite to that of the far field flow velocity U_0 [6]. The results of the present phase-field modeling also confirms this out-

come: with the imposing of the fluid flow, the growth becomes more pronounced in the opposite direction to the flow as shown in Fig. 1(b). For these structures, i. e. with the thermal noise in a stagnant melt and also with imposed flow of the melt (Fig. 1) we compared the results for dendrite growth velocity in pure nickel versus undercooling quantitatively.

The phase-field modeling exhibits an increase of the velocity of the up-stream dendritic branch in comparison with the dendrite tip velocity in a stagnant melt, Fig. 2. The enhanced dendrite velocity due to the melt flow has been found to decrease the disagreement between theory and experimental data, which is present at small undercoolings. Therefore we have compared quantitatively the predictions of the present phase-field modeling with the new experimental data [7] for growth kinetics of nickel dendrites.

7.3.2

Comparison with experimental data

We quantitatively analyzed the models predictions in comparison with previously recorded experimental data on dendritic solidification for nickel obtained with photodiode technique or, respectively, the capacitance proximity sensor (CPS) technique [1,2]. Particularly, it has been shown that the forced melt flow due to electromagnetic stirring in a droplet may increase the dendrite growth velocity if the flow imposed on the dendrite has the direction opposite to the growing dendritic tip [6]. However, the effect of the convective flow alone does still not explain the measured data in a satisfying manner. Therefore, to analyze critically the previous experimental data on dendritic growth, we improved the accuracy of the CPS technique and performed new measurements of dendritic growth velocities in levitated undercooled nickel samples [7]. The measurements were performed for dendritic growth velocity versus the amount of undercooling $T = T_L - T_\infty$ (where T_L is the liquidus temperature, and T_∞ is the actual temperature measured experimentally for the undercooled state of the liquid droplet in an electromagnetic levitation facility [17]). Solidification of the undercooled nickel melt was triggered at undercoolings in the range of $30 \text{ K} < \Delta T < 260 \text{ K}$. The new CPS data reveals high accuracy and low scattering, and showed in this investigation high reproducibility for six individual samples of different masses [7].

New experimental results for dendrite growth velocities in nickel are shown in Figure 2. Comparison of the model predictions, also shown in Fig. 2, with the new experimental results allows one to conclude that the predictions of the phase-field model, Eqs. (1)-(8), are partially agreeable to the experimental data. Particularly, the disagreement still exists in the range of undercooling $35 \text{ K} < \Delta T < 125 \text{ K}$, Fig. 2. Consequently, though the forced convection may drastically influence the thermal field around the growing dendrite and the growth kinetics itself, the disagreement between the modeling and experimental results still exists at small and, in part, moderate undercoolings.

The detailed analysis of the reasons of appearance of such a disagreement lead to the idea that tiny amounts of impurities may play a crucial role in the enhancement of the dendrite growth velocity at small undercoolings. A chemical analysis of the

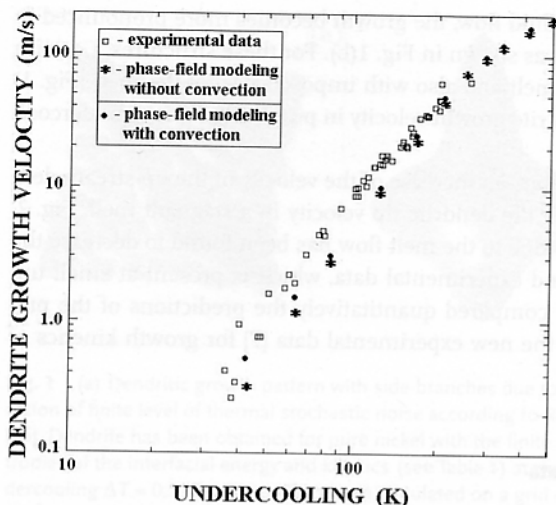


Fig. 2 Comparison of the results of the phase-field modeling for the dendrite tip velocity in stagnant melt, with the melt convection, and with the experimental data on growth kinetics of nickel dendrites. The new experimental data obtained using the improved CPS technique exhibits a smooth kinetic curve in comparison with the previous experimental data [7].

purity of samples used in for the new CPS measurements revealed that the amount of impurities is on the level of 0.01 at.% [7] which might play an essential role in the growth kinetics of nominally “pure” nickel [18]. Therefore we suggest on the basis of the current investigation that the influence of small amounts of impurities on the growth kinetics of nickel dendrites has the different temperature characteristic than of the effect by melt flow. This has allowed us to discriminate between both contributions as it is shown by experimental investigations and modeling within the sharp interface model [19] (for evaluation of the effect of solute diffusion) and the present phase-field modeling as well. The following analysis of these effects on the growth kinetics of nickel dendrites will be given elsewhere [20].

7.4 Conclusions

- (i) The results on phase-field modeling for dendritic growth with convective flow are presented. As the phase-field model predicts, the crystal structures are changing from grained crystals at small undercoolings up to grained crystals (with the planar smooth crystallographic grains) at higher undercoolings via the dendritic growth form within intermediate range. Within this range, the branched dendritic patterns occur, Fig. 1(a). With the fluid flow imposed on the growing dendrites, the crystal growth becomes more pronounced in the direction opposite to the flow, Fig. 1(b).

(ii) For comparison of the model predictions with experimental data, the new capacitance proximity sensor CPS data set on dendritic growth velocities in levitated undercooled nickel samples has been chosen [7]. A comparison of the results of the phase-field modeling with the new experimental results shows that though the forced convection may drastically influence on the thermal field around the growing dendrite and the growth kinetics itself, the disagreement between the modeling and experimental results still exists at small and, in part, moderate undercoolings, Fig. 2.

(iii) Very small amounts of impurities existing in nominally “pure” nickel samples may play an essential role in dendrite growth kinetics [7]. Due to the fact that the solute diffusion effect may show a different temperature characteristic than the transport effect by fluid flow, it is possible, as a first approximation, to discriminate between both these effects by investigating growth velocities as a function of undercooling [18]. Good agreement of the models predictions with experimental data on solidification of the nickel dendrites might be obtained when both effects of thermal convection and solute diffusion are taken into consideration [20].

Acknowledgements

We thank Christoph Beckermann and Georg Lohöfer for useful exchanges and discussions. Financial support of this work by Deutsche Forschungsgemeinschaft under the project No. HE 1601/13 is gratefully acknowledged.

References

- [1] E. SCHLEIP, R. WILLNECKER, D.M. HERLACH, G.P. Görler, Mater. Sci. Eng. 1988, 98, 39.
- [2] K. ECKLER, D.M. HERLACH, Mater. Sci. Eng. 1994, A178, 159.
- [3] D.M. MATSON, in Solidification 1998 (Ed.: S.P. Marsh, J.A. Dantzig, R. Trivedi, W. Hofmeister, M.G. Chu, E.J. Lavernia, J.-H. Chun), TMS, Warrendale PA, USA, 1998, p. 233.
- [4] J. LIPTON, M.E. GLICKSMAN, W. KURZ, Mater. Sci. Eng. 1984, 65, 57.
- [5] J. LIPTON, W. KURZ, R. TRIVEDI, Acta Metall. 1987, 35, 957.
- [6] P.K. GALENKO, O. FUNKE, J. WANG, D.M. HERLACH, Mater. Sci. Eng. A 2003, in press.
- [7] O. FUNKE, G. PHANIKUMAR, P.K. GALENKO, M. KOLBE, D.M. HERLACH, *New results on dendrite growth velocities during solidification of levitated undercooled Ni melts*, Physical Review E 2004, submitted.
- [8] L.Q. CHEN, Annu. Rev. Mater. Res. 2002, 32, 113.
- [9] W.J. BOETTINGER, J.A. WARREN, C. BECKERMANN, A. KARMA, Annu. Rev. Mater. Res. 2002, 32, 163.
- [10] A. KARMA, W.-J. RAPPEL, Phys. Rev. E 1996, 53, R3017.
- [11] A. KARMA, W.-J. RAPPEL, Phys. Rev. E 1998, 57, 4323.
- [12] J. BRAGARD, A. KARMA, Y. H. LEE, M. PLAPP, Interface Science 2002, 10(2–3), 121.
- [13] C. BECKERMANN, H.-J. DIEPERS, I. STEINBACH, A. KARMA, X. TONG, J. Comp. Physics 1999, 154, 468.
- [14] X. TONG, C. BECKERMANN, A. KARMA, Q. LI, Phys. Rev. E 2001, 63, 061601.
- [15] Y. LU, C. BECKERMANN, A. KARMA, Mat. Res. Soc. Symp. Proc. Vol. 701 MRS, USA, 2002, T2.2.1.

- [16] A. KARMA, W.-J. RAPPEL, Phys. Rev. E 1999, 60, 3614.
 - [17] D.M. HERLACH, Annu. Rev. Mater. Sci. 1991, 21, 23.
 - [18] D.M. HERLACH, O. FUNKE, G PHANIKUMAR, P.K. GALENKO, *Free dendrite growth in undercooled melts: experiments and modeling*. In: "TMS (The Minerals, Metals & Materials Society) Proceedings", 2004, accepted for publication.
 - [19] P.K. GALENKO, D.A. DANILOV, Phys. Lett. A 1997, 235, 271.
 - [20] P.K. GALENKO, D.M. HERLACH, O. FUNKE, G PHANIKUMAR, *Phase-field modeling of solidification of undercooled melt: a test and comparison for the current models with the new experimental data*, 2004, in preparation.